Nanoscale

PAPER

View Article Online
View Journal | View Issue

Cite this: *Nanoscale*, 2014, **6**, 13022

Tuning the molecular order of C_{60}-based self-assembled monolayers in field-effect transistors†

Thomas Schmaltz,[a] Artoem Khassanov,[a] Hans-Georg Steinrück,[b] Andreas Magerl,[b] Andreas Hirsch[c] and Marcus Halik*[a]

The control of order in organic semiconductor systems is crucial to achieve desired properties in electronic devices. We have studied the order in fullerene functionalized self-assembled monolayers by mixing the active molecules with supporting alkyl phosphonic acids of different chain length. By adjusting the length of the molecules, structural modifications of the alignment of the C_{60} head groups within the SAM can be tuned in a controlled way. These changes on the sub-nanometre scale were analysed by grazing incidence X-ray diffraction and X-ray reflectivity. To study the electron transport properties across these layers, self-assembled monolayer field-effect transistors (SAMFETs) were fabricated containing only the single fullerene monolayer as semiconductor. Electrical measurements revealed that a high 2D crystalline order is not the only important aspect. If the fullerene head groups are too confined by the supporting alkyl phosphonic acid molecules, defects in the crystalline C_{60} film, such as grain boundaries, start to strongly limit the charge transport properties. By close interpretation of the results of structural investigations and correlating them to the results of electrical characterization, an optimum chain length of the supporting alkyl phosphonic acids in the range of C_{10} was determined. With this study we show that minor changes in the order on the sub-nanometre scale, can strongly influence electronic properties of functional self-assembled monolayers.

Received 25th June 2014,
Accepted 1st September 2014

DOI: 10.1039/c4nr03557g

www.rsc.org/nanoscale

Introduction

Since a few years, organic electronic devices are emerging into the market. But to pave the way for further products, improvements in device performance have to be accomplished. Besides new materials, this requires a deeper understanding of the interplay between the active materials. Of particular significance in all electronic devices are interfaces between different layers – and to control the morphological and electronic structure of molecules at interfaces is the key challenge. A lot of work has been done to understand the correlation between chemical structure, thin film morphology and electrical properties of organic molecules at interfaces.[1–3] However, the ultimate goal is to design materials which form defined ordered structures *via* self-organization and thus ease the process to obtain desired properties. A good example are self-assembled monolayers (SAMs), which present an elegant approach to build thin films with defined thickness and structure, both determined by the molecular layout. The interactions between the surface and the anchor group of the molecules as well as the interactions between the molecules itself govern the morphology and thus the properties of such monolayers.[4] By varying the chemical structure of the SAM-forming molecules, complex functionalities can be achieved in monolayers. Examples are the tuning of surface energies over a wide range from superhydrophilic to superhydrophobic,[5,6] the adjustment of work functions[7,8] or to establish charge storing properties.[9] A further approach to tune surface properties is to mix different self-assembling molecules in solution, yielding mixed SAMs which typically exhibit properties in between those of the pure SAMs. By varying the mixing ratio, a continuous shift of the properties can be obtained, as exemplarily shown for the threshold voltage in organic thin film transistors.[10]

Due to this large variety in scope for design, SAMs have been successfully integrated into various organic electronic devices, such as organic thin film transistors (TFTs),[11,12] organic photovoltaics (OPV)[13] and organic memory devices.[9,14] Even semiconducting properties can be included in the molecules, which leads to organic semiconducting monolayers. These films can be incorporated as active layers in thin film

[a]*Organic Materials & Devices (OMD), Institute of Polymer Materials, University Erlangen-Nürnberg, Martensstraße 7, 91058 Erlangen, Germany. E-mail: marcus.halik@fau.de*
[b]*Crystallography and Structural Physics, University Erlangen-Nürnberg, Staudtstraße 3, 91058 Erlangen, Germany*
[c]*Department of Chemistry and Pharmacy, University Erlangen-Nürnberg, Henkestraße 42, 91054 Erlangen, Germany*

† Electronic supplementary information (ESI) available: Detailed results of GIDX, XRR and electrical measurements. See DOI: 10.1039/c4nr03557g

transistors, so called self-assembled monolayer field-effect transistors (SAMFETs).[15–20]

In these devices with real 2D-confined channels, the morphology is of particular interest, as small perturbations in the packing of the molecules, immediately strongly influence the transport properties in the transistor. This, on the other hand means that SAMFETs are an ideal tool to investigate thin film morphologies on the sub-nanometre scale in functionalized self-assembled monolayers.

In this work we investigate the tuning of molecular order in self-assembled monolayers of C_{60}-functionalized phosphonic acids and how electrical properties of these layers can be influenced in a controlled way. SAMs of functionalized fullerenes have been used in organic photovoltaics,[13,21,22] memory transistors,[9] light sensors[23] and SAMFETs.[18,24,25] In all of these devices the order of the SAM is of crucial importance for electronic properties. Therefore, ways to access information about and actually control the morphology of these films can enhance the device performance.

Previously, we reported on mixed SAMs with different mixing ratios of decylphosphonic acid (C_{10}-PA) and a fullerene functionalized alkylphosphonic acid ($C_{60}C_{18}$-PA, Fig. 1a). In simulations as well as experiments we found improved order and a positive effect on electronic properties in a broad range of mixing ratios, compared with the pure C_{60}-SAM, with an optimum mixing ratio around 1 : 1. Besides the mixing ratio, the structure of the supporting molecules can be expected to play a major role in terms of morphological control of the monolayer. Therefore, in this work we systematically varied the length of the alkyl chain of the supporting alkyl phosphonic acids from C_6 to C_{18} (Fig. 1a). Supporting molecules with alkyl chains longer than C_{18} are expected to be detrimental for the order, as the chain length of our active, C_{60} containing molecule is also C_{18}. A minimum chain length of C_6 was chosen to avoid etching of the AlO_x anchoring surface, as for decreasing length of alkyl-PAs the acidity increases.[26] To investigate the influence of the chain length of the supporting alkyl-PA on the morphology in the monolayer as well as the electronic properties, various analytical techniques were applied and SAMFET devices (schematic setup in Fig. 1b) were fabricated and electronically characterized. Grazing incidence X-ray diffraction (GIXD) was performed to obtain information about in plane order of the SAMs. X-ray reflectivity (XRR) measurements were conducted to access the out of plane structure of the monolayer that means in particular, the location of the C_{60}-moiety within the SAM. Monolayer transistors were fabricated in order to investigate the properties of such SAMs in real devices and – compared with the dimensions of the monolayer – over large areas of a few micrometres. A correlation between morphological results with electrical measurements can lead to a deeper understanding of what is important in such few nanometre thin films and how they can be tuned to feature desired properties.

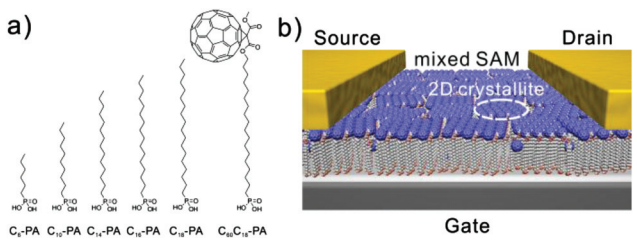

Fig. 1 (a) Chemical structures of the phosphonic acid molecules, which were used in the pure and mixed self-assembled monolayers. (b) Schematic image of a mixed alkyl-PA/C_{60}-functionalized-PA SAM in a SAMFET device.

Results and discussion

The self-assembly of monolayers of phosphonic acids on aluminium oxide (AlO_x) surfaces is an uncomplicated process which can be carried out from solution. In this work solutions of alkyl-PAs (C_6-PA, C_{10}-PA, C_{14}-PA, C_{16}-PA and C_{18}-PA) and $C_{60}C_{18}$-PA (Fig. 1a) were made in 2-propanol with a concentration of 0.005 mM. For self-assembly of mixed monolayers, the solutions of alkyl-PA and $C_{60}C_{18}$-PA were mixed in a 1 : 1-ratio, which is expected to result in roughly the same mixing ratio in the SAM.[24] For structural investigations, monolayers of respective mixtures of phosphonic acids were self-assembled on aluminium oxide (AlO_x) films of around 10 nm, grown by atomic layer deposition (ALD) on silicon substrates. These substrates offer an anchor surface which is very similar to the AlO_x in the SAMFET devices which is made by plasma oxidation of Al layers, yet much smoother which is crucial for the structural investigations. The self-assembled monolayers were prepared on these substrates in the same way as for the device fabrication (see Experimental).

Structural investigations

To get an insight into the nanoscale structure of these SAMs, grazing incidence X-ray diffraction (GIXD) as well as X-ray reflectivity (XRR) measurements were performed at the beamline ID10 at the European Synchrotron Radiation Facility (ESRF, Grenoble, France) using a wavelength of 0.56 Å.

GIXD measurements of all mixed and pure $C_{60}C_{18}$-PA SAMs resulted in three Bragg rods, which can be seen in the exemplary diffraction map in (q_r,q_z)-space of a C_{10}-PA/$C_{60}C_{18}$-PA SAM (Fig. 2a). The peaks become clearer in the profile (Fig. 2b) and were fitted with a Lorentzian that was convoluted with the resolution function (Fig. 2b, for more details see Experimental). Peak positions and the corresponding lattice spacing can be found in the ESI (Table S1†). These peaks can be attributed to the (10), (11) and (20) peak of a 2-dimensional hexagonal lattice (Fig. 2c). The nearest neighbour distance of 9.96 Å (±0.08 Å) corresponds nicely to the value which was found for C_{60} single crystals.[27] This means that the C_{60} head groups of the phosphonic acids form crystalline domains in the self-assembled monolayer, independently of whether the fullerene functionalized molecules are mixed with alkyl-PAs or not. The peak positions are the same for all mixed systems as well as for the pure $C_{60}C_{18}$-PA SAM, however the width of the peaks

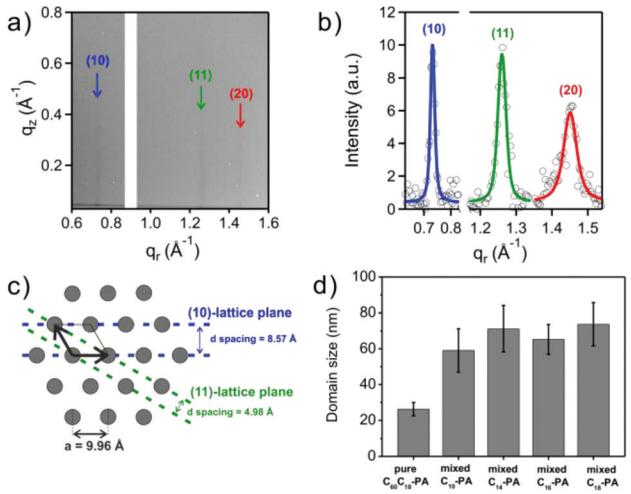

Fig. 2 Results of grazing incidence X-ray diffraction measurements on C_{60}-based SAMs with (a) diffraction map in (q_r,q_z)-space of a mixed C_{10}-PA/$C_{60}C_{18}$-PA SAM showing three Bragg rods; (b) extracted, background-corrected profile with the corresponding Lorentzian fits; (c) hexagonal crystal lattice with the measured d-spacing and the unit cell; (d) average domain sizes of the crystalline domains for the different SAMs.

differs. Using the Debye–Scherrer formula (see Experimental) we calculated the size of the C_{60} domains. Pure $C_{60}C_{18}$-PA SAMs exhibit domains with an average diameter below 30 nm, whereas all mixed alkyl-PA/$C_{60}C_{18}$-PA SAMs feature crystallite sizes of at least 60 nm (Fig. 2d). The alkyl-PAs in the mixed SAMs seem to push the C_{60}-moieties towards the surface and protect them from dunking into the SAM, thus enabling larger crystalline regions.

To analyse the vertical alignment, XRR measurements were carried out on the mixed alkyl-PA/$C_{60}C_{18}$-PA SAMs. The measured reflectivity data and the corresponding fits of a four slab model (AlO_x, anchor group, alkyl chain and C_{60} head group) are plotted in Fig. 3a. For details about the measurements and fitting procedure see Experimental part and ESI (Fig. S3†). From these fits the thickness, electron density and roughness of each individual slab can be obtained, which

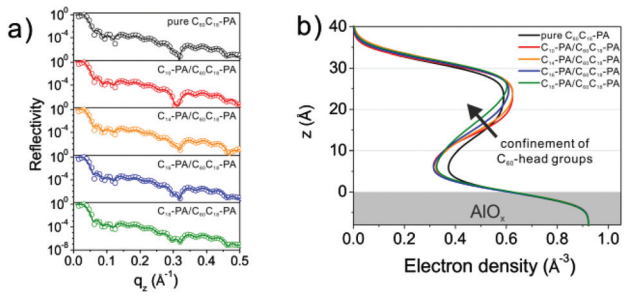

Fig. 3 (a) X-ray reflectivity data (circles) and corresponding fits (lines) for pure $C_{60}C_{18}$-PA and mixed alkyl-PA/$C_{60}C_{18}$-PA SAM systems; (b) corresponding electron density profiles of the SAMs, revealing an upholding effect of the alkyl-PAs for the C_{60}-moieties, which gets more pronounced for increasing length of the alkyl-PAs.

allows for close analysis of the vertical alignment of the self-assembled monolayers. Fig. 3b shows the vertical electron density distribution within our mixed SAMs. Starting from the ALD grown AlO_x with an electron density of 0.92 Å^{-3}, a decrease occurs at the anchor group and the alkyl chain of the SAMs. Further away from the substrate the electron density increases again and exhibits a broad peak, which corresponds to the fullerene head group, before the electron density drops to zero. This shape is similar for all SAMs; however, there are certain differences which point to structural differences between the systems. In the pure $C_{60}C_{18}$-PA SAM the electron density of the alkyl chain region is clearly higher than in case of the mixed SAMs. We interpret this as C_{60} head groups dunking into the SAM, possibly even as far down as to the AlO_x substrate. This is reasonable, due to the shape of the molecule with a slim alkyl chain and a comparably large fullerene head group. In the mixed SAMs this is prevented by the alkyl-PA molecules making up for the geometrically non-uniform framework of the $C_{60}C_{18}$-PA and filling out the space in between the alkyl chains of the functional molecules. Thus the alkyl-PAs push the C_{60} head groups upwards and lead to a confinement of the electron rich fullerenes within the monolayer. For increasing chain length of the alkyl-PAs, this effect gets more pronounced, which means the C_{60}-moieties on top of the alkyl chains are confined to a higher degree in a thin layer (with a thickness of one fullerene, *i.e.* 1 nm). This trend can be clearly seen in the electron density profiles (Fig. 3b), as the width of the C_{60} peak decreases and moves further away from the AlO_x substrate for increasing chain length of the supporting alkyl-PAs. Hence, alkyl-PAs with long chain length seem to increase the order in the C_{60}-based SAMs, by confining the active fullerene moieties in a thin film on top of the SAM.

Electrical results

Structural investigations revealed an improvement in molecular order – in plane as well as out of plane – for mixed alkyl-PA/$C_{60}C_{18}$-PA SAMs compared to the pure $C_{60}C_{18}$-PA, with a more pronounced confinement of the fullerenes for increasing alkyl chain length. Intuitively one would expect that the confinement of the C_{60}-moieties should lead to improvements in charge transport properties across those monolayers. To examine this hypothesis we fabricated SAMFET devices with mixed alkyl-PA/$C_{60}C_{18}$-PA SAMs as semiconducting layers with alkyl-PAs of chain length ranging from C_6 to C_{18}. On silicon substrates with 100 nm thermal SiO_2, aluminium gate electrodes were evaporated and lithographically patterned. An oxygen plasma treatment provided a thin aluminium oxide (AlO_x) film on top of the gate electrodes, acting as anchor surface for the phosphonic acids and simultaneously as dielectric. The monolayers were self-assembled from 2-propanol solutions on the AlO_x prior to source/drain electrode deposition and patterning. Details of the fabrication process are described in the Experimental. In contrast to recently reported results on C_{60}-based SAMFETs,[25] the transistors setup was slightly changed, which could lead to slightly different trends when directly comparing

results. In this work lithographically patterned top contacts were utilized, to allow for a high reproducibility of the gold source/drain contacts, due to the large injection area with the C_{60}-SAM. Furthermore, the top electrodes exclude contact related effects and enable the possibility to only investigate the charge transport across the SAMs. Proper ohmic contacts between the gold electrodes and the C_{60}-SAMs were obtained, indicated by the linear onset of the output characteristics of the transistors (ESI, Fig. S4†). This setup, however, requires bringing the active fullerene SAM into contact with both, the photoresist and acetone for the lift-off step. But neither the resist, which was spin-coated directly onto the C_{60}-SAM, nor the acetone seemed to deteriorate the electronic properties of the fullerenes. For all SAM systems at least seven transistors were characterized with channel length of around 3 μm and channel width of 100 μm. The capacitance for the mobility calculations was determined to 0.68 μF cm^{-2} ± 0.02 μF cm^{-2} (for details see Experimental) and employed for mobility calculations of all devices, due to only minor variations between the values for the different SAM systems.

Representative transfer curves of pure $C_{60}C_{18}$-PA, a mixed SAM with an alkyl-PA of medium chain length (C_{10}-PA) and a mixed SAM with an alkyl-PA of long chain length (C_{18}-PA) are plotted in Fig. 4a. Transfer curves of all SAM systems are shown in the ESI (Fig. S3a†). As expected, the mixed C_{10}-PA/$C_{60}C_{18}$-PA device outperforms the pure $C_{60}C_{18}$-PA SAMFET, but surprisingly the C_{18}-PA/$C_{60}C_{18}$-PA transistor exhibits a decreased performance compared to the other devices. To visualize a trend for all mixed systems, the average saturation mobility and drain current values are shown in Fig. 4b, plotted against the chain length of the supporting alkyl-PA (for pure $C_{60}C_{18}$-PA a supporting chain length value of zero was appointed). Mixing of $C_{60}C_{18}$-PA with alkyl-PAs of short to medium chain length leads to increased drain currents and charge carrier mobilities. Unexpectedly, this is not the case any more for longer chained alkyl-PAs (C_{14} and longer). Systematically the mobility and drain current values decrease with increasing chain length larger C_{10}. The same trend was found for on/off-ratios and drain current to leakage current ratios (I_D/I_G) in the devices (ESI – Fig. S3b†), as a consequence of the reduced drain current. This seems surprising, since the order of the functional C_{60}-moieties increases with increasing chain length, as shown before. But for charge transport, besides the 2D order of the semiconductor in the crystallites, the possibility to bridge over grain boundaries between the crystalline regions (≈60 nm) seems to be of great importance. The probability of this bridging, might be reduced by confining the fullerenes to a thin layer on top of the alkyl part of the SAM, leading to hindered charge transport across a large area, like the transistor channel. Therefore, a single monolayer of C_{60} is not essentially favourable, as soon as there are defects in the crystalline packing, such as grain boundaries. More favourable seems to be a crystalline C_{60} layer with a large enough number of underlying fullerenes, to increase the probability of electrical contact between individual crystallites. This appears to be the case in mixed SAMs with rather short chained alkyl-PAs, such as C_6-PA and C_{10}-PA. In the pure $C_{60}C_{18}$-PA a bridging also should be possible, but the fullerenes are not prevented from dunking deep down into the alkyl chain region of the SAM, where they are electronically isolated and thus not contributing to the charge transport. For charge transport across the SAM, mixed systems with short alkyl-PAs seems to be ideal, as they present a balance between supporting the fullerene head groups and simultaneously not confining them to a single layer, which enables a bridging between crystallites.

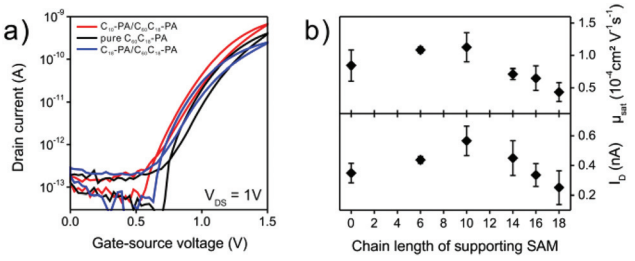

Fig. 4 Electrical results of C_{60}-based SAMFETs: (a) representative transfer curves of SAMFETs made of pure $C_{60}C_{18}$-PA, mixed C_{10}-PA/$C_{60}C_{18}$-PA and C_{18}-PA/$C_{60}C_{18}$-PA, respectively. (b) Average saturation mobilities and drain currents (from at least seven devices for each system) for all mixed alkyl-PA/$C_{60}C_{18}$-PA SAM systems (*x*-axis shows chain length of the alkyl-PA) and pure $C_{60}C_{18}$-PA devices (*x*-axis value of zero).

Experimental

Grazing incidence X-ray diffraction

Grazing Incidence X-ray Diffraction (GIXD) experiments were carried out at beamline ID10 at the European Synchrotron Radiation Facility in Grenoble using 22 keV X-rays. The impinging angle α was set to 0.080°, which is just below the critical angle of silicon, α_c = 0.082. The corresponding critical momentum transfer vector is q_c = 0.032 $Å^{-1}$. Thus the rays are totally externally reflected, and only the evanescent wave interacts with the sample. In this setup, the scattered intensity by the surface is maximized, whereas the bulk scattering is reduced to a minimum.[28,29] The data was collected with a *Pilatus 300K* area detector with an illumination time of 10 s. In this geometry, the momentum transfer vector $\boldsymbol{q}$ has a vertical and horizontal component, $q_z = 2\pi/\lambda(\sin\alpha + \sin\beta)$, where β is the outgoing angle, and $q_r \simeq 4\pi/\lambda(\sin 2\theta/2)$ respectively, where 2θ is the horizontal scattering angle.[30–32] Since the present self-assembled monolayers consist of crystallites, which are randomly oriented in the plane, any Bragg peak can be measured by mapping the $(2\theta, \beta)$-space.[33]

All peaks can be well described by a Lorentzian lineshape, $I(q_r) = \frac{I_0}{\pi}\frac{\kappa_r/2}{(q_r - q_0)^2 + (\kappa_r/2)^2}$. Such line shapes have already been successfully used to describe the scattering profiles of OTS self-assembled monolayer.[34] To obtain the intrinsic scattering widths, we have convoluted this profile with the Gaussian resolution function of the spectrometer. This analysis gives the peak position q_0 and a crystalline correlation

length, *i.e.* the size of the crystallites, which is related to the inverse of the full-width-half-maximum κ_r through the Debye–Scherrer formula $\xi \approx \frac{0.9 \times 2\pi}{\kappa_r}$.[35,36]

X-Ray reflectivity

Specular X-ray reflectivity (XRR) measurements were carried out at beamline ID10 at the European Synchrotron Radiation Facility in Grenoble using 22 keV X-rays. XRR was measured by scanning the detector, which was placed in the reflection plane, while keeping the outgoing angle β equal to incoming angle α with a scintillation detector and counting times of 0.3 s per point. In this geometry, the momentum transfer vector solely has a component normal to the surface, $q_z = 4\pi/\lambda \sin\alpha$. The reflected intensity was measured as a function of q_z, and was normalized to the incident intensity. The resulting reflectivity curves $R(q_z)$ are sensitive to the surface normal electron density profile and hence allow for independent determination of the thicknesses, electron densities and roughnesses of self-assembled monolayers with sub-Å resolution.[37–40] The surface normal electron density profile was simulated assuming 4 slabs of constant, but variable, electron density ρ_i, a thickness d_i and a Gaussian roughness σ_i. The individual slabs represent the ALD grown AlO_x, the phosphonic acid anchor group, the alkyl chain and the C_{60} functional head group. This profile was then substituted into the Abeles transfer matrix method using MOTOFIT.[41,42] The resulting reflectivity curve was subsequently least-square fit to the measured reflectivity data, yielding best values of ρ_i, d_i and σ_i. In the fitting routine the parameters for the ALD were fixed to common values for all samples.

TFT fabrication

Silicon wafer with 100 nm thermal SiO_2 served as smooth, insulating substrates for the SAMFET devices. Aluminium bottom gate electrodes (30 nm) were thermally evaporated at pressures below 10^{-6} mbar and patterned by photolithography and a standard lift-off process. After the lift-off in acetone, an oxygen plasma treatment was performed in a plasma chamber (Diener Electronic Pico, 200 W) for 5 min to generate a dense aluminium oxide layer of around 3.6 nm thickness.[43] This AlO_x film serves as inorganic part of the hybrid dielectric and as anchor surface for the phosphonic acids. The self-assembly of phosphonic acids on the surface was carried out directly after the plasma treatment by immersing the substrates into dilute solutions of $C_{60}C_{18}$-PA or mixed solutions of alkyl-PA (C_6-PA, C_{10}-PA, C_{14}-PA, C_{16}-PA or C_{18}-PA) and $C_{60}C_{18}$-PA in a 1 : 1 molar ratio with a overall concentration of 0.005 mM in 2-propanol. After 24 h the samples were removed from solution and thoroughly rinsed with 2-propanol and dried in a nitrogen stream. The photoresist (Microposit S1813) was spin-coated onto the SAM, exposed through a Cr mask with an UV-lamp and developed. Gold source and drain electrodes were thermally evaporated (30 nm) onto the substrate with the patterned resist and the lift-off process was performed in acetone. After the lift-off, the devices were transferred to a nitrogen flushed glovebox, annealed at 120 °C for approximately 16 h and electrically characterized. The capacitance, which was needed for the charge carrier mobility evaluation, was calculated in the same way as reported before,[20] using the capacitance value of an AlO_x dielectric, an estimated permittivity of an alkyl chain of 2.5 and the thickness of the alkyl-dominated part of the SAMs (measured by XRR). An average capacitance per area of 0.68 μF cm^{-2} ± 0.02 μF cm^{-2} was obtained and employed for all mobility calculations, due to the minor variations between the different SAM systems.

Conclusions

To summarize, mixed self-assembled monolayers of alkyl phosphonic acids and C_{60}-functionalized alkyl phosphonic acids were investigated with varying chain length of the alkyl-PAs. The influence of the supporting alkyl-PA molecules on the order of the C_{60} head groups in the layers was investigated by means of GIXD and XRR. GIXD measurements revealed crystalline packing of the fullerenes in a 2D hexagonal lattice in all SAM systems, but larger domain sizes for all mixed SAMs (≥60 nm) compared to the pure $C_{60}C_{18}$-PA SAM (<30 nm). XRR measurements showed an improved vertical alignment in mixed SAMs, by preventing fullerene head groups from dunking deep into the SAM and thus confining the C_{60} layer on top of the alkyl part of the SAM. This effect becomes more pronounced for alkyl-PAs with longer chains. The influence of tuning the order in the sub-nanometre scale of such films on the charge transport properties was investigated in self-assembled monolayer field-effect transistors. Such devices present an ideal system to characterize these 2D films, as they contain only a single, chemically bound layer of semiconductor. The expected improvement of the electronic properties in mixed SAMs was only validated for short alkyl-PAs up to chain length of C_{10}. Longer alkyl-PAs in the mixed SAMs led to a decrease in performance, which can be explained by closely analysing the results of the XRR measurements. By pushing the C_{60} head groups more and more away from the AlO_x substrate for growing chain length of the alkyl-PAs, the fullerenes are increasingly confined to a thin, single C_{60} layer. This hinders a charge transport in between crystalline regions, whereas in less confined layers a bridging between crystallites can occur *via* underlying fullerenes and maintain the charge transport even over defects, such as grain boundaries. The medium chain length of C_{10}-PA was found to exhibit the best balance between both effects, the increasing confinement of the C_{60} head groups at the SAM surface, while still offering the possibility of bridging between crystalline domains *via* underlying fullerene moieties.

Acknowledgements

We acknowledge gratefully the German Research Council (DFG), the Collaborative Research Centre 953, the Cluster of

Excellence "Engineering of Advanced Materials – EXC 315" (http://www.eam.uni-erlangen.de), the DFG research unit 1878, "Functional Molecular Structures on Complex Oxide Surfaces" and the Erlangen Graduate School of Molecular Science (GSMS) for financial support. We also acknowledge the European Synchrotron Radiation Facility for provision of synchrotron radiation facilities and we would like to thank Federico Zontone and Oleg Konovalov for assistance in using beamline ID10.

Notes and references

1 J. Veres, S. Ogier, G. Lloyd and D. De Leeuw, *Chem. Mater.*, 2004, **16**, 4543–4555.
2 N. Koch, *ChemPhysChem*, 2007, **8**, 1438–1455.
3 H. Dong, L. Jiang and W. Hu, *Phys. Chem. Chem. Phys.*, 2012, **14**, 14165–14180.
4 A. Ulman, *Chem. Rev.*, 1996, **96**, 1533–1554.
5 K. L. Prime and G. M. Whitesides, *Science*, 1991, **252**, 1164–1167.
6 Y. Jiang, Z. Wang, X. Yu, F. Shi, H. Xu, X. Zhang, M. Smet and W. Dehaen, *Langmuir*, 2005, **21**, 1986–1990.
7 B. de Boer, A. Hadipour, M. M. Mandoc, T. van Woudenbergh and P. W. M. Blom, *Adv. Mater.*, 2005, **17**, 621–625.
8 J.-P. Hong, A.-Y. Park, S. Lee, J. Kang, N. Shin and D. Y. Yoon, *Appl. Phys. Lett.*, 2008, **92**, 143311.
9 M. Burkhardt, A. Jedaa, M. Novak, A. Ebel, K. Voïtchovsky, F. Stellacci, A. Hirsch and M. Halik, *Adv. Mater.*, 2010, **22**, 2525–2528.
10 U. Zschieschang, F. Ante, M. Schlörholz, M. Schmidt, K. Kern and H. Klauk, *Adv. Mater.*, 2010, **22**, 4489–4493.
11 M. Halik, H. Klauk, U. Zschieschang, G. Schmid, C. Dehm, M. Schutz, S. Maisch, F. Effenberger, M. Brunnbauer and F. Stellacci, *Nature*, 2004, **431**, 963–966.
12 T. Sekitani, U. Zschieschang, H. Klauk and T. Someya, *Nat. Mater.*, 2010, **9**, 1015–1022.
13 T. Stubhan, M. Salinas, A. Ebel, F. C. Krebs, A. Hirsch, M. Halik and C. J. Brabec, *Adv. Energy Mater.*, 2012, **2**, 532–535.
14 T. Sekitani, T. Yokota, U. Zschieschang, H. Klauk, S. Bauer, K. Takeuchi, M. Takamiya, T. Sakurai and T. Someya, *Science*, 2009, **326**, 1516–1519.
15 G. S. Tulevski, Q. Miao, M. Fukuto, R. Abram, B. Ocko, R. Pindak, M. L. Steigerwald, C. R. Kagan and C. Nuckolls, *J. Am. Chem. Soc.*, 2004, **126**, 15048–15050.
16 M. Mottaghi, P. Lang, F. Rodriguez, A. Rumyantseva, A. Yassar, G. Horowitz, S. Lenfant, D. Tondelier and D. Vuillaume, *Adv. Funct. Mater.*, 2007, **17**, 597–604.
17 E. C. P. Smits, S. G. J. Mathijssen, P. A. van Hal, S. Setayesh, T. C. T. Geuns, K. A. H. A. Mutsaers, E. Cantatore, H. J. Wondergem, O. Werzer, R. Resel, M. Kemerink, S. Kirchmeyer, A. M. Muzafarov, S. A. Ponomarenko, B. de Boer, P. W. M. Blom and D. M. de Leeuw, *Nature*, 2008, **455**, 956–959.
18 M. Novak, A. Ebel, T. Meyer-Friedrichsen, A. Jedaa, B. F. Vieweg, G. Yang, K. Voitchovsky, F. Stellacci, E. Spiecker, A. Hirsch and M. Halik, *Nano Lett.*, 2011, **11**, 156–159.
19 A. Ringk, X. Li, F. Gholamrezaie, E. C. P. Smits, A. Neuhold, A. Moser, C. Van der Marel, G. H. Gelinck, R. Resel, D. M. de Leeuw and P. Strohriegl, *Adv. Funct. Mater.*, 2012, **23**, 2016–2023.
20 T. Schmaltz, A. Y. Amin, A. Khassanov, T. Meyer-Friedrichsen, H. G. Steinrück, A. Magerl, J. J. Segura, K. Voitchovsky, F. Stellacci and M. Halik, *Adv. Mater.*, 2013, **25**, 4511–4514.
21 S. K. Hau, H.-L. Yip, H. Ma and A. K.-Y. Jen, *Appl. Phys. Lett.*, 2008, **93**, 233304.
22 S. K. Hau, Y.-J. Cheng, H.-L. Yip, Y. Zhang, H. Ma and A. K. Y. Jen, *ACS Appl. Mater. Interfaces*, 2010, **2**, 1892–1902.
23 M. Salinas and M. Halik, *Appl. Phys. Lett.*, 2013, **102**, 203301.
24 A. Rumpel, M. Novak, J. Walter, B. Braunschweig, M. Halik and W. Peukert, *Langmuir*, 2011, **27**, 15016–15023.
25 C. M. Jaeger, T. Schmaltz, M. Novak, A. Khassanov, A. Vorobiev, M. Hennemann, A. Krause, H. Dietrich, D. Zahn, A. Hirsch, M. Halik and T. Clark, *J. Am. Chem. Soc.*, 2013, **135**, 4893–4900.
26 A. Jedaa, M. Burkhardt, U. Zschieschang, H. Klauk, D. Habich, G. Schmid and M. Halik, *Org. Electron.*, 2009, **10**, 1442–1447.
27 W. Kratschmer, L. D. Lamb, K. Fostiropoulos and D. R. Huffman, *Nature*, 1990, **347**, 354–358.
28 B. M. Ocko, X. Z. Wu, E. B. Sirota, S. K. Sinha, O. Gang and M. Deutsch, *Phys. Rev. E: Stat. Phys., Plasmas, Fluids, Relat. Interdiscip. Top.*, 1997, **55**, 3164–3182.
29 G. H. Vineyard, *Phys. Rev. B: Condens. Matter*, 1982, **26**, 4146–4159.
30 J. Als-Nielsen, D. Jacquemain, K. Kjaer, F. Leveiller, M. Lahav and L. Leiserowitz, *Phys. Rep.*, 1994, **246**, 251–313.
31 V. M. Kaganer, H. Möhwald and P. Dutta, *Rev. Mod. Phys.*, 1999, **71**, 779–819.
32 I. Kuzmenko, H. Rapaport, K. Kjaer, J. Als-Nielsen, I. Weissbuch, M. Lahav and L. Leiserowitz, *Chem. Rev.*, 2001, **101**, 1659–1696.
33 K. Kjaer, *Z. Phys. B: Condens. Matter*, 1994, **198**, 100–109.
34 I. M. Tidswell, T. A. Rabedeau, P. S. Pershan, S. D. Kosowsky, J. P. Folkers and G. M. Whitesides, *J. Chem. Phys.*, 1991, **95**, 2854–2861.
35 L. Tamam, H. Kraack, E. Sloutskin, B. M. Ocko and M. Deutsch, *Phys. Rev. B: Condens. Matter Mater. Phys.*, 2012, 85.
36 A. Guinier, *X-Ray Diffraction*, W.H. Freeman, 1963.
37 P. S. Pershan and M. Schlossman, *Liquid Surfaces and Interfaces: Synchrotron X-ray Methods*, Cambridge University Press, 2012.
38 M. Deutsch and B. Ocko, *Encyclopedia of Applied Physics*, VCH, New York 1998, vol. 23, pp. 479–490.
39 M. Tolan, *X-ray scattering from soft-matter thin films: materials science and basic research*, Springer, Berlin, 1999.
40 J. Als-Nielsen and D. McMorrow, *Elements of Modern X-ray Physics*, John Wiley and Sons, 2001.
41 A. Nelson, *J. Appl. Crystallogr.*, 2006, **39**, 273–276.
42 F. Abelès, *J. Phys. Radium*, 1950, **11**, 310–314.
43 M. Novak, T. Schmaltz, H. Faber and M. Halik, *Appl. Phys. Lett.*, 2011, **98**, 093302.